Wave Motion 75 (2017) 25–35

Contents lists available at ScienceDirect

Wave Motion

journal homepage: www.elsevier.com/locate/wamot

A method to recover water-wave profiles from pressure measurements

Vishal Vasan [a,*], Katie Oliveras [b], Diane Henderson [c], Bernard Deconinck [d]

[a] International Centre for Theoretical Sciences, Bengaluru, 560089, India
[b] Department of Mathematics, Seattle University, Seattle, WA 98122, United States
[c] Department of Mathematics, Pennsylvania State University, University Park, PA 16802, United States
[d] Department of Applied Mathematics, University of Washington, Seattle, WA 98195, United States

HIGHLIGHTS

- We propose a method to recover surface elevation profiles from pressure measurements.
- It is more accurate than traditional means for nonlinear traveling waves.
- It is as computationally efficient as linear theory.
- Experimental comparisons show the method works for interacting waves and wave groups.

ARTICLE INFO

Article history:
Received 11 February 2016
Received in revised form 4 July 2017
Accepted 8 August 2017
Available online 23 August 2017

Keywords:
Water waves
Pressure
Recovery
Measurement

ABSTRACT

An operational formulation is proposed for reconstructing a time series of water surface displacement from waves using measurements of pressure. The approach is based on the fully nonlinear formulation for pressure below traveling-wave solutions of Euler's equations developed by Oliveras, Vasan, Deconinck and Henderson. Its validity is tested using experiments in which both the pressure and the surface displacement are measured. The experiments include a wave system that is Galilean invariant – cnoidal waves, and wave systems that are not – reflected cnoidal waves and wave groups. We find that since the proposed formulation is nonlinear, it reproduces the amplitude spectrum of the measured surface displacements better than the hydrostatic model and better than the linear model that takes into account the pressure response factor due to small amplitude waves (the transfer function). Both the proposed formula and the transfer function reconstruct the surface reasonably well, with the proposed formula's being about 5% more accurate.

1. Introduction

Pressure transducers are a common device for measuring surface water waves in both the laboratory and the field. However, the inversion from pressure time series to surface displacement time series is nontrivial. The relationship between pressure and surface displacement, based on the Stokes boundary value problem [1], is nonlinear and involves fluid velocities. In practice, various approximate relationships are used. A common [2] relation between the surface displacement spectrum S_f and the pressure spectrum S_p is

$$S_f = NS_p/K_p, \tag{1}$$

* Corresponding author.
E-mail address: vishal.vasan@icts.res.in (V. Vasan).

http://dx.doi.org/10.1016/j.wavemoti.2017.08.003
0165-2125/

where N is an empirical factor, and

$$K_p = \frac{\cosh k(h+z)}{\cosh kh} \tag{2}$$

is the pressure response factor, which is obtained from linear theory and takes into account pressure due to wave motion. Here, h is the water depth; k is the radian wavenumber related to radian wave frequency ω through the linear dispersion relation $\omega^2 = gk\tanh(kh)$; g is the acceleration of gravity and $z < 0$ is the vertical depth of the pressure transducer, measured positive upward from the still water level. The empirical factor $N = 1$ corresponds to linear wave theory. The conventional wisdom from the Shore Protection Manual [2] is that N decreases with decreasing period; $N > 1$ for long-period waves, and $N < 1$ for short-period waves.

There have been many field and laboratory studies to determine if linear theory provides an adequate relationship between pressure measurements and surface displacement, and some disagreement exists. Bishop & Donelan [3] reviewed these studies. They concluded that linear wave theory is adequate for obtaining surface wave heights from pressure gage data to within 5%, except when measuring waves in shallow water. For waves in shallow water, they concurred with [4] that one must use $N \neq 1$ in order to account for currents and wave nonlinearity. Also energy from higher frequency waves is not recovered adequately by (1) because the higher frequency velocities fall off rapidly with increasing depth, because of inherent limitations of the pressure transducers and because of spectral leakage to high frequencies due to the form of K_p.

Tsai et al. [5] reviewed efforts to include nonlinear effects through Stokes expansions, some of which showed improvement over linear theory and some of which did not. They concluded both that "These seemingly incoherent results in fact only reflect the different wave conditions being studied". and that "... it is universally understood that the non linear correction is essential in shallow water or in surf zone". See [6] for references to alternative approaches including empirical models and neural networks. Fully nonlinear models for surface displacement recovery based on the equations for traveling water waves were presented in [6–10]. The subject remains an area of importance and on-going work. Indeed, the array of about 40 DART (Deep-ocean Assessment and Reporting of Tsunamis) buoys used for obtaining real-time surface-displacement data for tsunami forecasting rely on pressure measurements, as do measurements of storm surge from hurricanes [11].

In this paper, we address the need for obtaining an operational nonlinear mapping from pressure to surface displacement following Oliveras *et al.* [6]. Rather than starting with the Stokes boundary value problem and proceeding with a perturbation expansion in the surface displacement and velocity potential, we in [6] started with a reformulation of the Stokes boundary value problem given by [12]. From this representation, we found an exact formulation for the surface displacement that requires the numerical solution of a nonlocal, nonlinear equation. The errors with respect to nonlinearity do not exceed machine precision. In addition, we also found an approximation of the full formula, which we propose for operational use here.

In the formulation in [6], we made two key assumptions. The first assumption is that the pressure transducers are situated at the bottom of the fluid domain. However, many of the papers discussed above, such as [13], have shown that the transducer is often not at the bottom, but at some point in the water column. In recent work by two of the authors, this limitation was overcome. In [14] the authors show how surface reconstruction is possible from pressure data obtained at any depth below the free surface. The second key assumption is that surface displacements are due to a traveling solitary wave system. In the current work we present results from a set of experiments designed to test the limits of the theory developed in [6]. Here we report on experimental comparisons with predictions to see if the proposed formula works for wave systems that break the assumption of a traveling wave system. The experimental apparatus is presented in Section 3. Results are presented in Section 4 for experiments that use cnoidal waves, which give a periodic, traveling wave system as assumed by the theory, and for experiments that use reflecting cnoidal waves and wave groups, neither of which comprise traveling wave systems. We summarize results in Section 5.

Our main conclusion is that since the proposed formula (16) is nonlinear, it reproduces the amplitude spectrum of the measured surface displacements better than does the transfer function (1) with the empirical constant $N = 1$. The experiments show that both the proposed formula (16) and the transfer function reconstruct the surface displacement reasonably well, with predictions from (16) being about 5% more accurate. Hence, we claim that the proposed formula (16) presented here provides a better mapping from time series measurements of pressure to time series of surface displacement than is otherwise available. It is more accurate than (1), requires just one more Fourier transform, is no less general because of the assumption of traveling waves, and it can include an arbitrary depth for the pressure transducer.

2. Theory

Here we review our theoretical approach from [6] in which we derived the proposed formula (Section 2.1) in the context of solitary traveling water waves. Next, we modify the theory for the case of periodic traveling waves and follow this with a discussion on three particular reduced models for reconstruction of surface elevation. In recent work the authors extend the theory to allow for pressure measurements obtained at arbitrary depths [14].

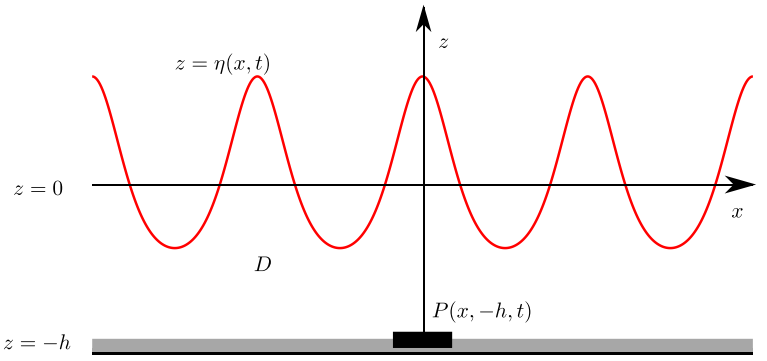

Fig. 1. The fluid domain D. A pressure sensor is indicated at the bottom. In our calculations the pressure measurement is assumed to be a point measurement.

2.1. Preliminaries

Consider Euler's equations describing the dynamics of the surface of an ideal irrotational fluid in two dimensions (with a one-dimensional surface):

$$\phi_{xx} + \phi_{zz} = 0, \qquad (x,z) \in D, \tag{3}$$

$$\phi_z = 0, \qquad z = -h, \tag{4}$$

$$\eta_t + \eta_x \phi_x = \phi_z, \qquad z = \eta(x,t), \tag{5}$$

$$\phi_t + \frac{1}{2}\left(\phi_x^2 + \phi_z^2\right) + g\eta = 0, \qquad z = \eta(x,t), \tag{6}$$

where $\phi(x,z,t)$ represents the velocity potential of the fluid with surface elevation $\eta(x,t)$. A solution to the above set of equations consists of finding a potential ϕ that satisfies Laplace's equation inside the fluid domain D, sketched in Fig. 1, as well as finding the graph of the free surface η. Below we pose the problem on the whole line $x \in \mathbb{R}$, assuming the velocities (and surface profile) decay at infinity.

Our goal is to relate the pressure measured at a sensor $P(x_0, -h, t)$, which is also sketched in Fig. 1, located on the bottom boundary of the fluid, to the surface elevation profile $\eta(x_0, t)$. Eqs. (3)–(6) do not involve the pressure field. However, the pressure can be introduced through the Bernoulli condition, which is valid in the interior of the fluid:

$$\phi_t + \frac{1}{2}\left(\phi_x^2 + \phi_z^2\right) + gz + \frac{P(x,z,t)}{\rho} = 0, \quad -h \le z \le \eta(x,t). \tag{7}$$

The overall scheme is as follows. Since (7)) is valid at the bottom boundary, we employ it to convert the pressure measurement into a condition on the velocity potential at $z = -h$. In addition, we note from Eqs. (5)–(6), that the velocity potential at the surface is related to the surface elevation profile. Since the potential ϕ satisfies Laplace's equation, the boundary values of the potential at $z = -h$ and $z = \eta$ must be related. This consistency of boundary values forms the basis of our reconstruction method.

The scheme described in the previous paragraph involves connecting boundary data at the bottom and top surfaces. Setting $\phi_z(x, -h, t) = 0$ in Eq. (7) we obtain a relation between the bottom pressure $P(x, -h, t)$ and $\phi(x, -h, t)$. A major difficulty in the problem of surface reconstruction, however, is that the input data is typically a time series of the pressure at $z = -h$ for a single spatial point (or discrete set of points), *i.e.*, $P_j(x_j, -h, t)$, $j = 0, 1, 2, \ldots$, where x_j need not be spaced close together. Therefore, we require a method to convert $P(x_j, -h, t)$ to $P(x, -h, t)$ for a given j. Further, having recovered $P(x, -h, t)$, we seek $\phi(x, -h, t)$ through (7). We claim this is not practical without further simplification. To see why, consider (7) as a partial differential equation for $\phi(x, -h, t)$ with $P(x, -h, t)$ as a forcing term. Evidently we require knowledge of an initial state for $\phi(x, -h, t)$, *i.e.*, an initial condition.

In the following, we restrict to the case of a traveling wave moving with velocity c. This assumption permits us to translate time series data to spatial information, establishes the initial state of the fluid (indeed the state for all time) and permits the study of nonlinear effects. The inclusion of nonlinear effects increases the accuracy of surface reconstruction. Of course, assuming a traveling wave comes at a cost. The speed of the wave is required to translate the time series data to a spatial measurement.

The main result of [6] is the establishment of the following nonlinear, nonlocal relationship between the non-static pressure at the bottom boundary and the surface elevation profile of a traveling wave solution to Euler's equation. Indeed if we assume both ϕ and η depend on the horizontal coordinate x and time t through the combination $\xi = x - ct$, where c is

the speed of the traveling wave, the equations of motion are now given as

$$\Phi_{\xi\xi} + \Phi_{zz} = 0, \qquad (x, z) \in D, \tag{8}$$

$$\Phi_z = 0, \qquad z = -h, \tag{9}$$

$$-c\eta_\xi + \eta_\xi \Phi_\xi = \Phi_z, \qquad z = \eta(\xi), \tag{10}$$

$$-c\Phi_\xi + \frac{1}{2}\left(\Phi_\xi^2 + \Phi_z^2\right) + g\eta = 0, \qquad z = \eta(\xi), \tag{11}$$

where $\Phi(\xi, z) = \phi(x, z, t)$. The Bernoulli condition at $z = -h$ is given as

$$-c\Phi_\xi + \frac{1}{2}\Phi_\xi^2 - gh + \frac{P(\xi, -h)}{\rho} = 0. \tag{12}$$

Denoting by $p(\xi)$ the non-static part of the pressure at the bottom in the traveling coordinate frame, scaled by the fluid density: $p(\xi) = -gh + P(\xi, -h)/\rho$, in [6], we obtain the relationship

$$\sqrt{\frac{c^2 - 2g\eta}{1 + \eta_\xi^2}} = \frac{1}{2\pi}\int_{-\infty}^{\infty} e^{ik\xi} \cosh\left(k\left(\eta + h\right)\right) \mathcal{F}\left\{\sqrt{c^2 - 2p}\right\}(k)\, dk, \tag{13}$$

where $\mathcal{F}$ denotes the Fourier transform: $\mathcal{F}\{y(\xi)\}(k) = \int_{-\infty}^{\infty} y(\xi)\exp(-ik\xi)d\xi$.

2.2. Reconstruction of periodic wave profiles

For the case of periodic traveling wave profiles, one obtains an arbitrary constant of integration denoted by B on the right-hand side of the Bernoulli condition (11) as well as (12). The quantity c^2 in Eq. (13) is then replaced by $F = c^2 + 2B$. When the vertical coordinate is chosen so that the surface elevation η has average zero, then F is a non-negative number referred to as the Bernoulli constant. The wave speed c is defined as the vertical average of the horizontal velocity. Then the speed c is the speed of the wave in a frame of reference where there is no mean flow.

It would appear that the reconstruction formula depends on the Bernoulli constant F. In [15] the authors investigated the dependence on the Bernoulli constant F for the reconstruction algorithm using numerically computed traveling water wave solutions to Euler's equations. They found that the method introduced in [6] was particularly insensitive to errors in the wave speed. From a practical standpoint, using only time series of pressure at individual locations, it is not possible to measure or estimate F. Since we seek to develop an operational formula, we wish to avoid requiring any knowledge of F. Consequently, we limit the discussion in the current work to asymptotic formulas derived from (13) that are independent of F. Thus for the conversion from $P(x, -h, t_0) \to \eta(x, t_0)$, in the current work, we employ three $F-$independent reconstruction formulas obtained from the fully nonlinear method of [6]. They are the hydrostatic model, the transfer function and the proposed formula (16). Two of these asymptotic reductions are standard models discussed in Section 1: the hydrostatic approximation

$$\eta = \frac{p}{g}, \tag{14}$$

and the transfer function (1) with the empirical constant $N = 1$, which gives a linear, dynamic correction to the hydrostatic approximation;

$$\mathcal{F}[\eta] = \cosh(kh)\mathcal{F}\left[\frac{p}{g}\right]. \tag{15}$$

The third is the proposed model

$$\eta = \frac{\mathcal{F}^{-1}\left[\cosh(kh)\mathcal{F}\left[\frac{p}{g}\right]\right]}{1 - \mathcal{F}^{-1}\left[k\sinh(kh)\mathcal{F}\left[\frac{p}{g}\right]\right]}, \tag{16}$$

which yields the best results of all of the reduced models in the comparisons reported in [6]. We call (16) the "heuristic model".

Eq. (16) is derived as a nonlinear correction to (15) in the context of traveling waves [6]. However, the transfer function (15) has a dual interpretation since it can be derived either in the time dependent context (by linearizing the original equations of motion) or in the traveling wave context (from the full nonlocal nonlinear result (13)). Thus one is tempted to view (16) as a correction to (15) even in the context of time dependent flows. Indeed the experiments suggest this correction is relevant to generic, time-dependent, shallow-water surface profile reconstruction.

2.3. The role of wave-speed

From an operational standpoint, one does not have access to $P(x, -h, t_0)$ which is a measurement of the bottom pressure at all horizontal locations. Indeed, the output from the pressure and surface gauges consisted of a time series of the pressure

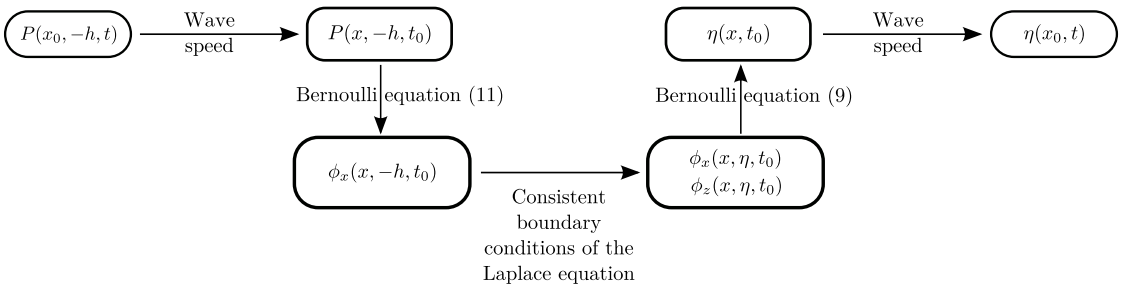

Fig. 2. Summary of the surface reconstruction algorithm.

and surface displacement at a fixed location respectively. The theory for surface reconstruction, however, is based on knowledge of the pressure field, *i.e.*, a spatial measurement. This necessitates a conversion from the given time series to a spatial measurement, followed by the reconstruction procedure of [6]. A pictographic overview of this process is shown in Fig. 2. For the reconstruction methods considered in the current work, the Bernoulli constant does not appear in the reconstruction of $\eta(x, t_0)$ from $P(x, -h, t_0)$, *i.e.*, the central part of Fig. 2. However, one does require a wave speed to convert the time series of pressure measurements to a spatially extended measurement.

The choice of wave speed depends on the particular type of wave. We note that all models considered herein require knowledge of wave speed, since all models make a spatial reconstruction out of temporal measurements. This is consistent with practical use of the transfer function in the field. In the current work we consider three types of waves: periodic traveling waves, wave groups and reflected waves. For periodic traveling waves we use the speed of the wave in the lab frame of reference. This was measured by noting the arrival time of the crest of the wave at two consecutive pressure measurement stations. The reflected waves are generated by periodic traveling waves that are reflected off the end of the tank. In this case also, we use the speed of the wave as measured in the lab. Thus in both these cases $\omega = c_w k$ is the relation employed to convert a time series into a spatial measurement, where c_w is the speed of the wave. In the case of wave groups, we use the (uni-directional) linear dispersion relation $\omega = \sqrt{gk \tanh(kh)}$ to relate frequencies and wave numbers.

3. Experimental apparatus and procedure

Experiments were conducted in the William G. Pritchard Fluid Mechanics Laboratory in the Department of Mathematics at Pennsylvania State University to create and measure a variety of waves for comparisons of surface reconstructions using the three models (14)–(16). In these experiments the pressure at the bottom of the fluid and the displacement of the air–water interface were measured simultaneously during wave propagation.

3.1. Apparatus

The wave tank is 50 ft long and 10 inches wide with tempered glass walls and bottom. It was cleaned with alcohol and filled with tap water to a depth greater than the desired depth, h, so that the surface could be cleaned. We cleaned the surface using a fan attached to one side of the tank. It blew a wind that created a surface current that carried contaminants attached to the surface along the length of the tank to the other end (50 ft away). There we used a wet vac to vacuum the contaminants along with the top few millimeters of fluid. We used a Lory Type C point gage to measure the resulting water depth h.

We used two types of wave gages: a capacitance gage for measuring surface displacements directly and a pressure transducer mounted into a hole in the bottom glass panel. The pressure transducer was a SEN^{Z}ORS PL6T submersible level transducer with a range of 0–4 in. It provided a 0–5 V dc output, which was digitized with an NI PCI-6229 analog-to-digital converter using LabView software. We calibrated this transducer by raising and lowering the water level in the channel. The pressure measurements had a high-frequency noise component, and thus low-pass filters were employed.

We implemented two possible low-pass filters. In the first case, by averaging the Fourier amplitudes of the high-frequency wave numbers we estimated a noise level. All modes with Fourier amplitudes less than or equal to this noise level were set to zero. The noise level was chosen so that the transform $\cosh(kh)$ resulted in a smooth reconstruction. Effectively, this filter picked out the dominant modes. In the second case, the pressure measurements were filtered assuming a suitable cut-off frequency. For instance, data from a measurement of a 1 Hz cnoidal wave was filtered with a cut-off frequency of 10 Hz. This smoothing however does not necessarily regularize the hyperbolic transforms employed in the transfer and heuristic function approach. To do so we replaced the original hyperbolic terms with $\cosh(\alpha kh)$ and $\sinh(\alpha kh)$, where $\alpha = 1$ if $kh < 1$ and $\alpha = 0$ otherwise. Thus when $\alpha = 0$, both transfer and heuristic functions are equivalent to the identity map. In essence, we wish to apply the recovery algorithm only to the shallow water component of the measured signal.

Both low-pass filters produced qualitatively similar results in real space. Further, the frequency corresponding to $kh = 1$ was close to the largest dominant mode picked out by the first method. In the experiments discussed below this was around 2

Hz. The heuristic function, being a nonlinear map from pressure to surface elevation, introduces higher wave number modes into the reconstruction unlike the transfer function approach. The first method of filtering typically retains a small number of dominant modes and so is ideally suited to understanding the nonlinear interactions generated by the heuristic function. However, in practice, we prefer the second method of filtering the pressure measurements since it is physically motivated and relatively simple to implement.

The capacitance-type surface wave gage consisted of a conducting wire coated with the commercially available super-hydrophobic coating "Rustoleum's NeverWet". The coated wire was connected to two quartz crystals. One had a fixed oscillation frequency and one had a frequency dependent on the water height on the coated wire. The difference frequency was read by a Field Programmable Gate Array (FPGA), NI PCI-7833R. The surface capacitance gage was held in a rack on wheels that was attached to a programmable belt. We calibrated the capacitance gage by traversing the rack at a known speed over a precisely machined, trapezoidally-shaped "speed bump". Time series of surface displacement were obtained using LabView software that controlled the FPGA board.

3.2. Wave generation

The waves were generated with a piston-type paddle made from Teflon and machined to fit the channel with a thin lip around its periphery that served as a wiper with the channel's glass perimeter. This wiper minimized leakage around the paddle during paddle motion. The paddle was attached to a Parker 406 LXR linear motor, controlled using the Aries Controller Program (ACR) 6 software. The motion of this paddle could be precisely programmed to provide a smooth stroke profile with a resolution of 1/42000 inch. In order to perform controlled and repeatable experiments, we generated specific known surface profiles. We adopt the approach of [16] to prescribe the motion of the paddle $L(t)$ using a conservation of mass principle leading to the following equation for L in terms of the wave profile η

$$\frac{dL}{dt} = \frac{1}{\eta(L(t), t) + h} \int_{L(t)}^{\infty} \eta_t \, dx. \tag{17}$$

In the following, we derive the associated forcing equation for certain classes of target profiles.

1. **Periodic traveling waves**: Here we take

$$\eta = \begin{cases} f(x - ct), & x - ct \geq \xi_0, \\ \zeta(x - ct), & x - ct < \xi_0, \end{cases}$$

where $\zeta(\xi)$ is a target profile, $f(\xi)$ is a traveling front that vanishes as $\xi \to \infty$ and $\xi_0 > L(t)$ for all t. Substituting this form for η into (17) we obtain

$$\frac{dL}{dt} = \frac{c\,\zeta(L - ct)}{\zeta(L - ct) + h}. \tag{18}$$

The periodic waves generated here are KdV cnoidal waves (particular periodic solutions of the Korteweg de Vries equation), such that (see [17])

$$\zeta(\xi) = t_0 + a_0 \mathrm{cn}^2\left(\frac{2K(m)\xi}{\lambda}, m\right), \tag{19}$$

where a_0 is the trough-to-crest height of the wave, m is the elliptic modulus [18,19], $K(m)$ is the complete elliptic integral of the first kind [18,19], t_0 is the trough level and λ is the wavelength. Given a_0, the frequency f_0 and mean depth of fluid h, one obtains the remaining quantities from the following relationships:

$$\begin{aligned} t_0 &= \frac{a_0}{h}\left(1 - m - \frac{E(m)}{K(m)}\right), \\ \lambda &= h\sqrt{\frac{16}{3}\frac{mh}{a_0}}K(m), \\ c &= \sqrt{gh}\left[1 + \frac{a_0}{mh}\left(1 - \frac{m}{2} - \frac{3E(m)}{2K(m)}\right)\right], \\ c &= \lambda f_0, \end{aligned}$$

where $E(m)$ is the complete elliptic integral of the second kind [18,19], c is the speed of the wave and g is the acceleration due to gravity. Combining the last three equations above, one obtains the elliptic modulus using a simple Newton's method.

2. **Reflected waves**: Reflected cnoidal waves were generated when the cnoidal wave train generated as described above reached the end of the wave tank and reflected. Measurement stations for surface height and bottom pressure were the same in the case of a single traveling wave. The reflected wave had the same speed as the original wave but in the opposite direction.

3. **Wave group**: A wave packet is produced by considering a target profile of the form $\zeta = \zeta_1 + \zeta_2$ where $\zeta_i = A\sin(k_i x - w_i t)$. Here $|w_1 - w_2|$ is small and k_i is obtained by solving the linear dispersion relation $w_i^2 = gk_i \tanh(k_i h)$. Thus the amplitude should be small enough such that the linear approximation is valid. Under these assumptions, the differential equation for $L(t)$, (18), has a similar form as in the previous cases, with the numerator's on the right-hand side being $c_1\zeta_1 + c_2\zeta_2$ with $c_i = w_i/k_i$.

We wish to emphasize that the case of reflected waves and wave groups is outside of the purview of the original theory developed in [6]. In the following section we present reconstruction of such wave profiles using the hydrostatic, transfer function and heuristic formula approaches. Aside from the translation of time series into spatial measurement (as described in Section 2.3), the formulas were applied with no additional adjustments.

4. Results and discussions

We use measurements of time series of pressure measured at a point at the bottom of the wave tank to reconstruct the corresponding time series of the surface displacement. We compare the reconstruction with direct measurements of the surface displacement. The theory assumes that the wave fields are traveling waves. In previous work we showed comparisons for solitary wave forms modeled by KdV solitons [6]. Here we look at the periodic case by generating KdV cnoidal waves. In order to see how the theory works for more realistic shallow-water conditions, we also look at wave systems outside the range of validity of the theory, including reflected cnoidal waves, and wave groups. In the comparisons below we define the transfer function approach to be the one obtained from linear water-wave theory. This is equivalent to (15), which is (1) with the empirical constant $N = 1$.

4.1. Cnoidal waves

To look at the reconstruction for periodic waves, we generated a cnoidal wave, (19) using a frequency of $f_0 = 1$ Hz and crest-to-trough height of $a_0 = 1.9$ cm in water with quiescent depth $h = 6.16$ cm as discussed in Section 3. The speed of the cnoidal wave profile was within 0.5% of the shallow water speed $\sqrt{gh}$, where g is the acceleration due to gravity. We note that because of dissipation the measured wave amplitudes do not agree with the amplitude programmed at the wavemaker.

Fig. 3 shows results. The measured time series is shown in Fig. 3(a)–3(c) along with reconstructions using the hydrostatic approximation (14), the transfer function (15) that accounts for linear wave motion, and the heuristic model (16) obtained from the fully nonlinear model in [6]. We note that in the troughs, the measured time series has a bump that is not captured by the hydrostatic or transfer functions, and only slightly captured by the heuristic model. The source of this bump in the experiments is the contact line between the cnoidal wave crest and the glass sidewalls. The interaction there results in a short-crested wave at symmetric angles from both sidewalls. They intersect in the trough of the cnoidal wave and look like an inverse Kelvin wake.

Overall, we see that in this experiment, the hydrostatic approximation is the least accurate, while the transfer and heuristic models agree reasonably well with the measurements; the heuristic model is more accurate than the transfer function in capturing the peak amplitude. Another test of the models is to look at their Fourier amplitudes. Fig. 3(d) shows the ratio of predicted to measured Fourier amplitude, with predictions from the transfer and heuristic models. An amplitude ratio of 1 corresponds to agreement between measurements and model predictions. Overall, the heuristic formula computes Fourier amplitudes closer to the true value. However, the predictions of transfer function and heuristic formula agree at certain frequencies (as seen by the overlapping gray and black dots in Fig. 3(d)). In the reconstructions, one must pick a wavenumber cut-off for the Fourier transforms because of the factor of $\cosh(kh)$ that appears in the transfer function and the heuristic formula. This cut-off is clear in the ratio of Fourier amplitudes for the transfer function (shown by the gray dots in Fig. 3(d)) and occurs at about 2.5 Hz. Below this frequency, transfer and heuristic predictions agree. However, the nonlinearity in the heuristic formula (shown by the black, dashed curve in Fig. 3(d)) allows for nonlinear interactions among Fourier modes, so that it fills in the spectrum regardless of the cut-off. Note that transfer and heuristic reconstructions still agree at alternating frequencies above the cut-off where the transfer function is identically zero (up to machine precision).

4.2. Reflected cnoidal waves

In this section and in Section 4.3, we discuss experiments that push the assumptions of the theory. Such an approach is not new. Indeed, the hydrostatic formula (14) is employed even when fluid velocities are non-zero. Similarly, the transfer function (15) is strictly valid only for infinitesimally small wave amplitudes and yet still finds considerable use in practical situations. In the field, waves are reflected by beaches, other topographic features and man-made fixtures. To see if the theory presented here, which assumes traveling waves (necessarily in one direction) works in this regime, even though it is outside the range of validity of the theory, we did experiments using cnoidal waves that were generated at one end of the tank, as described in Section 3.2 and allowed to reflect off the wall at the other end of the tank. Below we present results for a cnoidal wave generated with $f_0 = 1$ Hz, $a_0 = 1.9$ cm and $h = 6.16$ cm.

Fig. 4 shows results. The measured time series is shown in Fig. 4(a)–4(c) along with reconstructions using the hydrostatic approximation (14), the transfer function (15) that accounts for linear wave motion, and the heuristic model (16) obtained from the fully nonlinear model in [6].

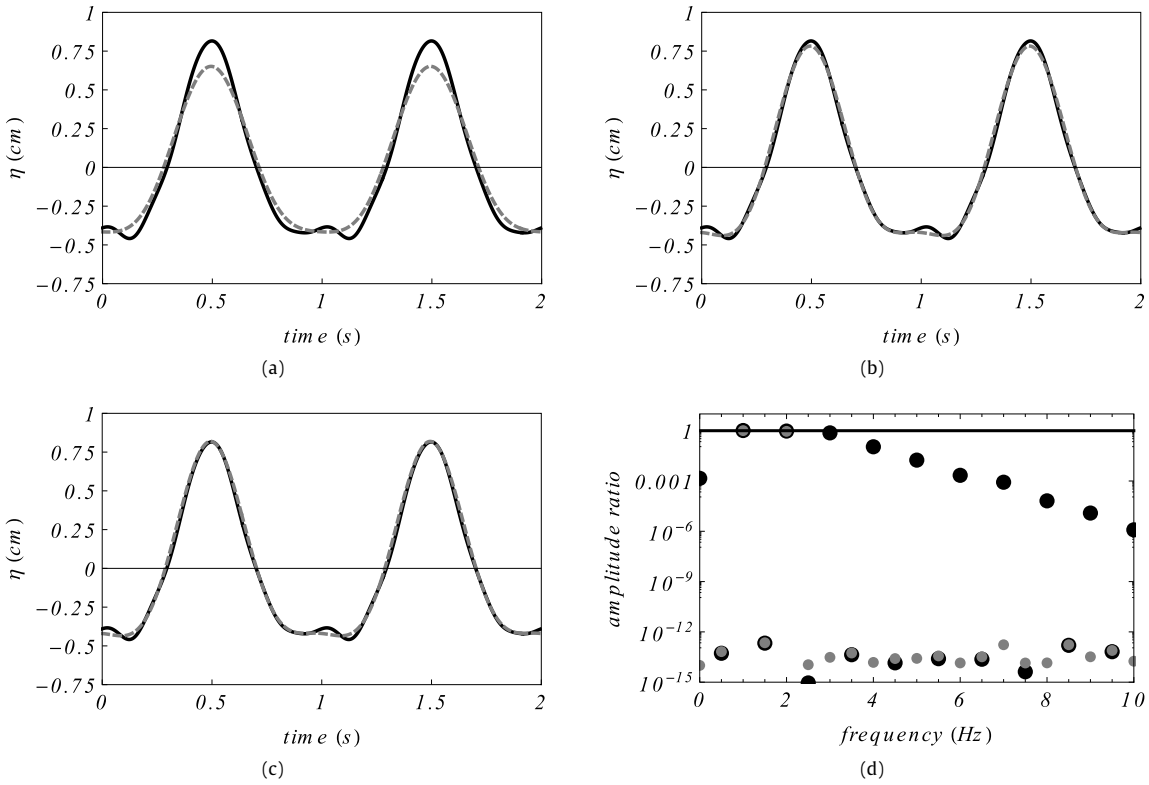

Fig. 3. Reconstruction of cnoidal waves. (a–c) Time series of measured and reconstructed surface displacements. Measurements are shown by the solid black curve. The dashed, gray curve represents: (a) the hydrostatic approximation, (14); (b) the transfer function, (15); (c) the heuristic formula, (16); (d) The ratio of the Fourier amplitudes of the reconstructed elevation to the measured elevation for the transfer function (gray dots) and heuristic formula (black dots). The solid black line shows the spectral goal of a successful reconstruction.

Overall, we see that in this experiment, the hydrostatic approximation is the least accurate. The transfer and heuristic models are in reasonable agreement with the measurements of the surface displacements, with the heuristic formula performing best overall. As discussed in Section 4.1, the Fourier amplitudes provide further information. Fig. 4(d) shows the ratio of predicted to measured Fourier amplitude, with predictions from the transfer and heuristic models. Again, the wavenumber cut-off for the Fourier transforms due to the factor of $\cosh(kh)$ that appears in the transfer function and the heuristic formula occurs at about 8 Hz. The reconstruction using the transfer function has negligible energy in frequencies above this cut-off, while the heuristic formula, due to its allowance for nonlinear interactions, has energy in the higher frequency modes, as does the spectrum from the measurements.

4.3. Wave groups

When swell approaches shallow water from deep water, it typically arrives in wave groups. Again, wave groups are outside the range of validity of the present theory, which assumes that all waves travel at a single speed. However, we did comparisons with wave groups, which were generated as discussed in Section 3.2. Here we used $A = 0.5$ in, $\omega_1 = 2\pi$ s^{-1}, and $|\omega_1 - \omega_2| = 0.1 \cdot 2\pi$ s^{-1}. The results are shown in Fig. 5.

All of the three models considered capture the phasing of the individual waves correctly. Again, the hydrostatic approximation underestimates the wave amplitudes, while the transfer and heuristic models are in reasonable agreement with the measurements of the surface displacements. The heuristic formula performs best overall. As before, the spectrum shows that the nonlinear coupling of modes allowed in the heuristic formula generates energy at modes above the cut-off for analysis; so the energy spectrum obtained from the heuristic formula is much closer to that of the measured spectrum than is that of the transfer function.

5. Summary

We have proposed alternative formulas to the standard hydrostatic approximation and transfer function for reconstructing a wave surface that is measured using a pressure transducer. These formulas are approximations and extensions to the

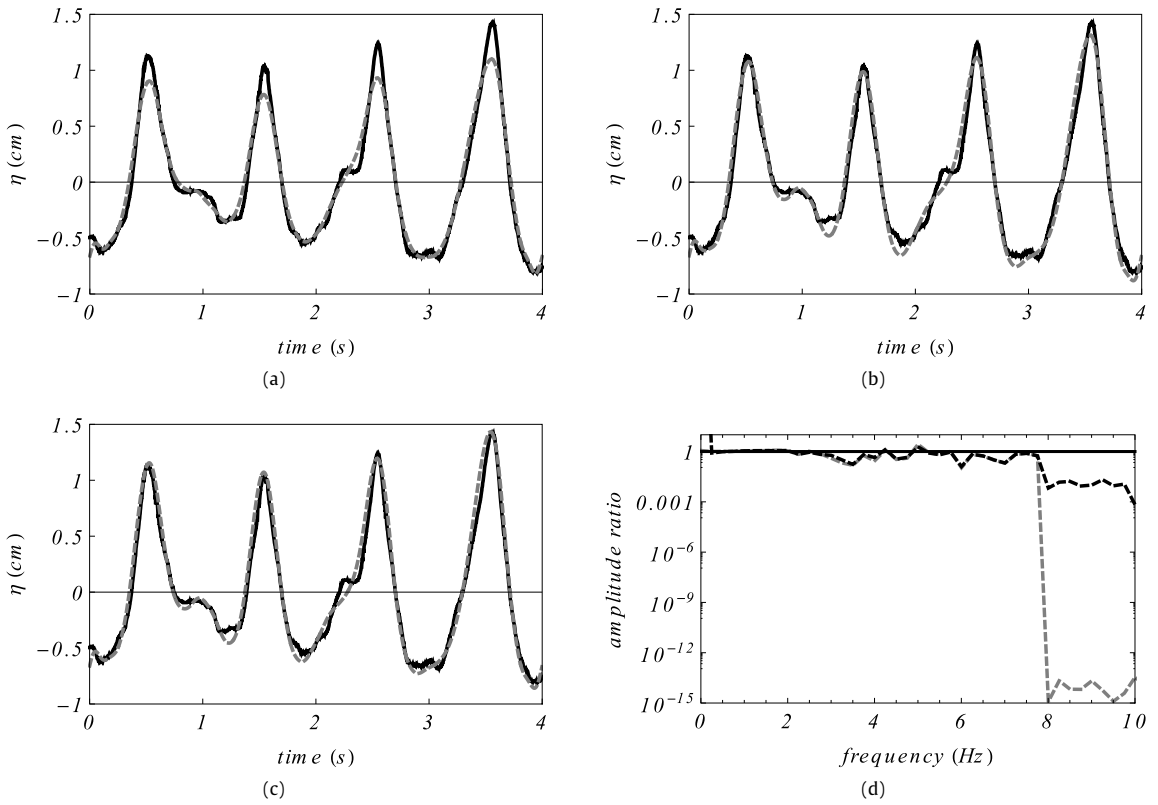

Fig. 4. Reconstruction of reflected cnoidal waves. (a–c) Time series of measured and reconstructed surface displacements. Measurements are shown by the solid black curve. The dashed, gray curve represents: (a) the hydrostatic approximation, (14); (b) the transfer function, (15); (c) the heuristic formula, (16); (d) The ratio of the Fourier amplitudes of the reconstructed elevation to the measured elevation for the transfer function (dashed, gray curve) and heuristic formula (dashed, black curve). The solid black line shows the spectral goal of a successful reconstruction.

fully nonlinear, non-local formulas derived by [6] that assumes traveling waves. If the transducer is at the bottom of the water column, then one can approximate the water surface displacement using the heuristic formula

$$\eta = \frac{\mathcal{F}^{-1}\left[\cosh(kh)\mathcal{F}\left[\frac{p}{g}\right]\right]}{1-\mathcal{F}^{-1}\left[k\sinh(kh)\mathcal{F}\left[\frac{p}{g}\right]\right]},$$

which is (16). In a recent paper [14] we extended the above result to the case when pressure is not measured at the bottom of the water column. If the pressure transducer is at a depth of $|z_0|$ from the still water surface, then one first uses the pressure measurements at this depth, p_0, to find the pressure at the bottom using

$$\mathcal{F}[p] = \operatorname{sech}(k(h-z_0))\mathcal{F}[p_0]\,.$$

Then one applies the heuristic formula above given by (16).

In [6], we tested the fully nonlinear theory and various approximations with measurements of solitons and found that, other than the fully nonlinear model, the heuristic formula gave the best agreement with measurements. Here we compared reconstructions using the hydrostatic approximation (14), the transfer function (15) and the heuristic formula (16) with measurements of (periodic) cnoidal waves and with two wave systems that are outside the range of validity of the theory: reflected cnoidal waves and wave groups. We found that since the heuristic formula includes nonlinearity, its amplitude spectrum more closely approximates that of the surface data. The hydrostatic approximation is inadequate in reconstructing the measured time series, while both the transfer and heuristic formulas reproduce it reasonably well. Nevertheless, in a comparison of the heuristic and transfer functions, we note that the heuristic formula gives results that are consistently about 5% more accurate and the spectrum of the heuristic formula consistently more accurately describes that of the data. The heuristic formula is straightforward to use, requiring just one more Fourier transform than the transfer function. Further, the assumption of traveling waves, which is inherent in both the heuristic formula and transfer function, does not seem to be a limiting factor in accuracy. Thus, we conclude that the heuristic formula provides a better inverse map of pressure measurements to surface displacement than does the transfer function.

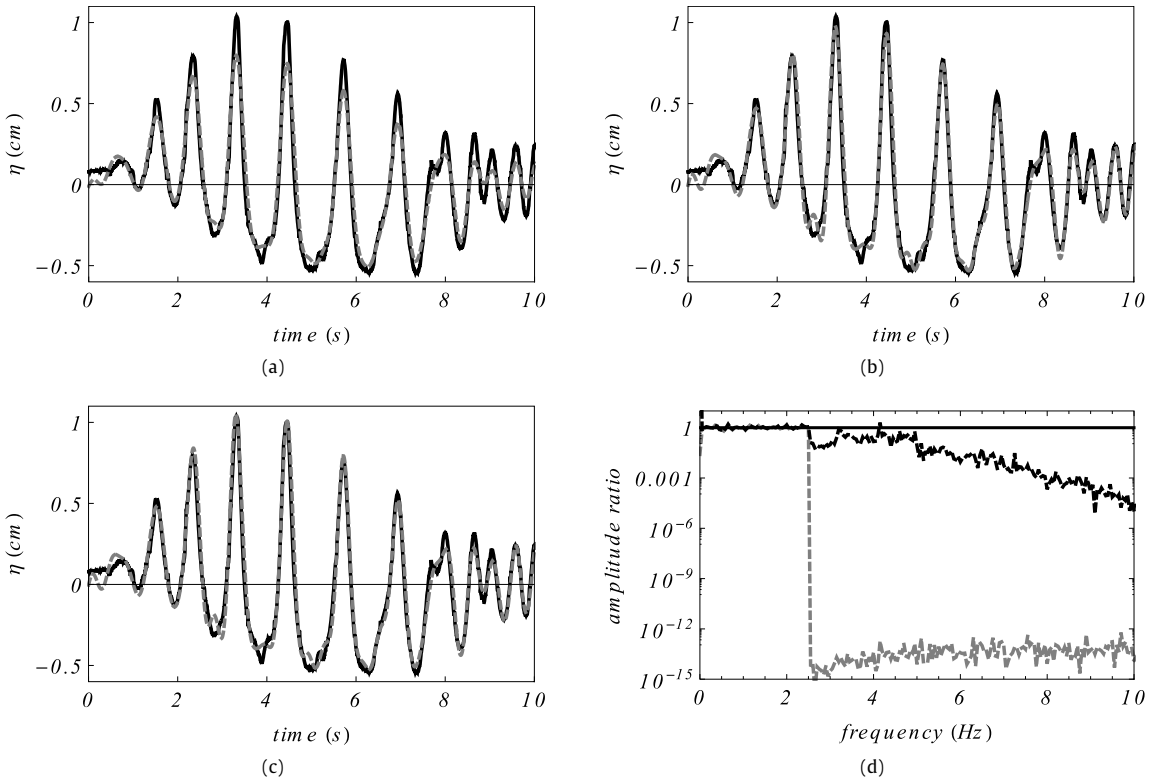

Fig. 5. Reconstruction of a wave group. (a–c) Time series of measured and reconstructed surface displacements. Measurements are shown by the solid black curve. The dashed, gray curve represents: (a) the hydrostatic approximation, (14); (b) the transfer function, (15); (c) the heuristic formula, (16); (d) The ratio of the Fourier amplitudes of the reconstructed elevation to the measured elevation for the transfer function (dashed, gray curve) and heuristic formula (dashed, black curve). The solid black line shows the spectral goal of a successful reconstruction.

Acknowledgments

This work was completed while the authors were in residence at the Institute for Computational and Experimental Research in Mathematics (ICERM) in Providence, RI, during the Spring 2017 semester. The ICERM semester was supported by the National Science Foundation under Grant No. DMS-143978. There they also had helpful discussions with Didier Clamond. BD and VV acknowledge support from the National Science Foundation under grant NSF-DMS-1008001. DH acknowledges support from the National Science Foundation under grants NSF-DMS-0708352 and NSF-DMS-1107379. KO gratefully acknowledges support from the National Science Foundation under grant DMS-1313049 and AMS-Simons Travel Grant. We thank Robert Geist for construction of the laboratory apparatus and Rod Kreuger for building the FPGA wave gage system. Any opinions, findings, and conclusions or recommendations expressed in this material are those of the authors and do not necessarily reflect the views of the funding sources.

References

[1] G. Stokes, Mathematical and Physical Papers, Vol. 1, Johnson Reprint Corp., NY & London, 1966.
[2] U.A.E.W.E. Station, Shore Protection Manual, Vol. 1m, fourth ed., 1984, Vicksburg Miss MI.
[3] C.T. Bishop, M.A. Donelan, Measuring waves with pressure transducers, Coast. Eng. 11 (1987) 309–328.
[4] D.Y. Lee, H. Wang, Measurement of surface waves from subsurface guage, 1984.
[5] C.-H. Tsai, M.-C. Huang, F.-J. Young, Y.-C. Lin, H.-W. Li, On the recovery of surface wave by pressure transfer function, Ocean Eng. 32 (2005) 1247–1259.
[6] K. Oliveras, V. Vasan, B. Deconinck, D. Henderson, Recovering the water-wave profile from pressure measurements, SIAM J. Appl. Math. 72 (2012) 897–918.
[7] D. Clamond, A. Constantin, Recovery of steady periodic wave profiles from pressure measurements at the bed, J. Fluid Mech. 714 (2013) 463–475.
[8] A. Constantin, On the recovery of solitary wave profiles from pressure measurements, J. Fluid Mech. 699 (2012) 1–9.
[9] H.-C. Hsu, Recovering surface profiles of solitary waves on a uniform stream from pressure measurements, DCDS-A 34 (2014) 3035–3043.
[10] D. Clamond, New exact relations for easy recovery of steady wave profiles from bottom pressure measurements, J. Fluid Mech. 726 (2013) 547–558.
[11] A.B. Kennedy, R. Gravois, B. Zachry, R. Luettich, T. Whipple, R. Weaver, J. Reynolds-Fleming, Q.J. Chen, R. Avissar, Rapidly installed temporary gauging for hurrican waves and surge, and application to hurricane gustav, Cont. Shelf Res. 30 (2010) 1743–1752.
[12] M.J. Ablowitz, A.S. Fokas, Z.H. Musslimani, On a new non-local formulation of water waves, J. Fluid Mech. 562 (2006) 313–343.

[13] J.-Y. Chen, Three dimensional nonlinear pressure transfer function, Coast. Eng. 11111 (2000) 3111109–3111128.
[14] V. Vasan, K. Oliveras, Water-wave profiles from pressure measurements: extensions, Appl. Math. Lett. 68 (2017) 175–180.
[15] B. Deconinck, K.L. Oliveras, V. Vasan, Relating the bottom pressure and the surface elevation in the water wave problem, J. Nonlinear Math. Phys. 19 (Suppl. 1) (2012) 1240014, 11.
[16] D.G. Goring, F. Raichlen, The generation of long waves in the laboratory, in: Proc. 17th Intl. Conf. Coastal Engrs. Sydney, Australia 11111, 1980, pp. 3111109–3111128.
[17] M.W. Dingemans, Water Wave Propagation over Uneven Bottoms, World Scientific, 1997.
[18] NIST Digital Library of Mathematical Functions, http://dlmf.nist.gov/, Release 109 of 2014-08-29, online companion to [19]. URL http://dlmf.nist.gov/.
[19] F.W.J. Olver, D.W. Lozier, R.F. Boisvert, C.W. Clark (Eds.), NIST Handbook of Mathematical Functions, Cambridge University Press, New York, NY, 2010 print companion to [18].